Mon. Not. R. Astron. Soc. **368,** 1735–1741 (2006) doi:10.1111/j.1365-2966.2006.10240.x

Can the unresolved X-ray background be explained by the emission from the optically-detected faint galaxies of the GOODS project?

M. A. Worsley,[1⋆] A. C. Fabian,[1⋆] F. E. Bauer,[2] D. M. Alexander,[1] W. N. Brandt[3] and B. D. Lehmer[3]

[1]*Institute of Astronomy, Madingley Road, Cambridge CB3 0HA*
[2]*Department of Astronomy, Columbia University, 538 W 120th Street, New York, NY 10027, USA*
[3]*Department of Astronomy and Astrophysics, 525 Davey Laboratory, Pennsylvania State University, University Park, PA 16802, USA*

Accepted 2006 February 22. Received 2006 February 18; in original form 2005 April 25

ABSTRACT

The emission from individual X-ray sources in the *Chandra* Deep Fields and *XMM–Newton* Lockman Hole shows that almost half of the hard X-ray background above 6 keV is unresolved and implies the existence of a missing population of heavily obscured active galactic nuclei (AGN). We have stacked the 0.5–8 keV X-ray emission from optical sources in the Great Observatories Origins Deep Survey (GOODS; which covers the *Chandra* Deep Fields) to determine whether these galaxies, which are individually undetected in X-rays, are hosting the hypothesized missing AGN. In the 0.5–6 keV energy range, the stacked-source emission corresponds to the remaining 10–20 per cent of the total background – the fraction that has not been resolved by *Chandra*. The spectrum of the stacked emission is consistent with starburst activity or weak AGN emission. In the 6–8 keV band, we find that upper limits to the stacked X-ray intensity from the GOODS galaxies are consistent with the ∼40 per cent of the total background that remains unresolved, but further selection refinement is required to identify the X-ray sources and confirm their contribution.

Key words: surveys – galaxies: active – galaxies: starburst – X-rays: diffuse background – X-rays: galaxies.

1 INTRODUCTION

Most of the extragalactic X-ray background (XRB) has been conclusively shown to be the integrated emission from discrete sources, in particular, the accretion light from active galactic nuclei (AGN). The 1–10 keV XRB has a spectral slope of $\Gamma = 1.4$ with a 5–10 per cent spread in measurements of the normalization (see e.g. Revnivtsev et al. 2003; De Luca & Molendi 2004), a large amount of which is due to field-to-field variations (Barcons, Mateos & Ceballos 2000). Emission from sources resolved by *Chandra* in the broad 0.5–2 keV and 2–10 keV bands is able to account for 80–90 per cent of the XRB (Mushotzky et al. 2000; Giacconi et al. 2002; Alexander et al. 2003a; Bauer et al. 2004), leading to some claims that the origin of the background has been solved. Recent analysis of very hard (>5 keV) X-ray data, however, as well as growing evidence from infrared (IR) and submillimetre studies, indicate that a substantial number of hard X-ray emitting AGN may remain to be found.

Although the resolved XRB in the broad 2–10 keV range is high, this does not imply that the background is accounted for at 10 keV, since the fraction is dominated by counts in the 2–6 keV range to which telescopes such as *Chandra* are most sensitive (Worsley et al. 2005). Narrow energy-band source-stacking in the *XMM–Newton* Lockman Hole (*XMM*-LH) and *Chandra* Deep Fields-North (CDF-N) and South (CDF-S) indicates that the resolved fraction of the XRB decreases from ∼80–90 per cent over 2–8 keV, to ∼60 per cent over 6–8 keV, and only ∼50 per cent > 8 keV (Worsley et al. 2004, 2005). These analyses derived the resolved fraction by summing, in narrow energy bands, the X-ray fluxes from all individually detected sources. The same source list was used for each narrow band considered, regardless of whether or not a source is explicitly detected in that band (most, but not all, sources were actually detected in the soft $\lesssim$2 keV range; refer to Worsley et al. 2004, 2005, and references therein). The unresolved background component has a spectral shape that is consistent with an unresolved population of highly obscured AGN at redshifts ∼0.5–1.5 and with absorption column densities of $\sim 10^{23}$–5×10^{24} cm^{-2}. Since the sources have not been individually detected in X-rays, their intrinsic, de-absorbed luminosities are probably $\lesssim 5 \times 10^{43}$ erg s^{-1} (rest-frame 2–10 keV), though this depends on important assumptions about their space density and absorption column densities.

The steeply rising X-ray source number counts in the 5–10 keV band show no evidence for flattening towards fainter fluxes (Hasinger et al. 2001; Baldi et al. 2002; Rosati et al. 2002). Since the

⋆E-mail: maw@ast.cam.ac.uk (MAW); acf@ast.cam.ac.uk (ACF)

average spectral slope of sources is known to be a strong function of flux – becoming progressively harder with decreasing flux (Ueda et al. 1999; Alexander et al. 2003a; Fiore et al. 2003; Streblyanska et al. 2004) – this also suggests a large, undiscovered population of faint, hard X-ray sources.

Locally, highly obscured AGN outnumber their unobscured counterparts by a factor of ∼4:1. The three nearest luminous AGN – Cen A, NGC 4945 and Circinus – all have column densities $>10^{23}$ cm^{-2}, with NCG 4945 and the Circinus galaxy being Compton thick (Matt et al. 2000). Population-synthesis models (e.g. Gilli, Salvati & Hasinger 2001; Franceschini, Braito & Fadda 2002; Gandhi & Fabian 2003; Ueda et al. 2003; Comastri 2004) require large numbers of highly obscured AGN in order to account for the 30-keV peak in the XRB spectrum (Setti & Woltjer 1989). If the ratio of obscured to unobscured AGN remains high (e.g. Gilli et al. 2001 predicted the ratio to be 10:1) out to high redshift, then a large number of faint, obscured sources could remain undetected in deep X-ray observations. At redshifts $z \gtrsim 1$, recent, careful studies suggest that the ratio of obscured to unobscured AGN is indeed high (e.g. Alexander et al. 2005 find ∼6:1).

Highly obscured AGN can show little or no soft X-ray emission due to photoelectric absorption, particularly if the covering fraction of the obscuring material is high and the fraction of reflected light is low. Current X-ray telescopes have been able to detect many low-redshift obscured AGN, as well as examples of type II quasars (e.g. Norman et al. 2002; Stern et al. 2002; Gandhi et al. 2004), yet sensitivity to faint, hard sources is still limited. Highly obscured sources with Seyfert luminosities (e.g. the Circinus galaxy) are undetectable even in the CDFs beyond redshifts of 0.2–1 (see fig. 6 in Brandt & Hasinger 2005) – the distance at which the majority of unobscured AGN are found. Submillimetre and IR observations (see e.g. Alexander et al. 2003b, 2005; Treister et al. 2004), may be the key to identifying the highly absorbed sources through the reprocessed AGN emission emerging at these wavelengths. IR colour selection using the *Spitzer* data should be able to disentangle starburst emission from the re-radiated AGN emission (Alonso-Herrero et al. 2004; Lacy et al. 2004, 2005).

The Great Observatories Origins Deep Survey (GOODS) (Dickinson et al. 2003) is an ongoing campaign of multiwavelength deep-field observations composed of existing and planned surveys. The programme is being carried out in two fields, each ∼10 × 16 arcmin^2 in size. The GOODS North (GOODS-N) field is contained within the ∼2 Ms CDF-N (Alexander et al. 2003a) and includes the *Hubble Deep Field* North (Williams et al. 1996; Ferguson, Dickinson & Williams 2000). The GOODS South (GOODS-S) field lies inside the ∼ 1 Ms CDF-S (Giacconi et al. 2002) and contains the *Hubble Space Telescope* (*HST*) *Ultra Deep Field* observation. As part of the GOODS project, the *Spitzer Space Telescope* has also carried out deep-IR surveys in the region from 3.6 to 24 μm (PI M. Dickinson) and the *HST* Advanced Camera for Surveys (ACS) has provided deep imaging of the fields in four broad wavebands (Giavalisco et al. 2004), not to mention a host of observations from ground-based telescopes.

We have performed X-ray stacking of optically-detected GOODS galaxies that have not been individually detected in X-rays: we specifically ignore all the X-ray sources that have already been individually detected in the CDFs – stacking analyses of these objects are covered in our earlier work (see Worsley et al. 2005). Since the GOODS probes optical galaxies to low luminosity and high redshift, once the already-detected X-ray sources are removed, the remaining 'normal' galaxies are likely candidates to host the hypothesized missing population of highly obscured AGN.

2 ANALYSIS

2.1 X-ray data and optically-detected sources

The 1.95-Ms CDF-N covers a total of 447.8 arcmin^2 and is larger than the GOODS-N optical survey region, which is focused on the CDF-N aim-point. 3σ X-ray source detection sensitivities are $\sim 2.5 \times 10^{-17}$ and $\sim 1.4 \times 10^{-16}$ erg cm^{-2} s^{-1} in the 0.5–2 and 2–8 keV bands, respectively. We use the main point-source catalogue (see Alexander et al. 2003a) which contains 503 sources. The 0.94-Ms CDF-S is also larger than the GOODS-S optical region with an area of 391.3 arcmin^2 and detection sensitivities of $\sim 5.2 \times 10^{-17}$ and $\sim 2.8 \times 10^{-16}$ erg cm^{-2} s^{-1} in the 0.5–2 and 2–8 keV bands, respectively. The main point-source catalogue contains 326 sources (Alexander et al. 2003a).

The deep optical imaging of the GOODS regions, using the *HST* ACS is now available in the four non-overlapping photometric filters: *F435W* (B_{435}), *F606W* (V_{606}), *F775W* (i_{775}) and *F850LP* (z_{850}) (Giavalisco et al. 2004). The 5σ limiting magnitudes in these four bands are 27.9, 28.2, 27.5 and 27.4, respectively (assuming an aperture of 0.5 arcsec). We use the r1.1z version of the GOODS ACS catalogue[1] which contains 32 048 and 29 661 optically-detected sources in the entire GOODS-N and GOODS-S regions, respectively.

2.2 X-ray image stacking

Our stacking procedure is similar to that taken by Lehmer et al. (2005) (also see Brandt et al. 2001; Nandra et al. 2002). At each optical source position we extract photon counts from the X-ray images and exposure times from the X-ray exposure maps. We used circular extraction apertures where a fixed 3-pixel radius (1.476 arcsec) was found to give the best signal-to-noise ratio (S/N) compared to 2- and 4-pixel apertures. To avoid contamination by X-ray detected sources, we did not stack any optical sources lying within three times the 90 per cent encircled-energy fraction radius of an X-ray source (Alexander et al. 2003a). We performed our stacking procedure in several narrow energy bands: 0.5–1, 1–2, 2–4, 4–6 and 6–8 keV.

The background was estimated using a Monte Carlo approach. Each stacking position was randomly shifted in RA and Dec. up to 60 arcsec away from its original position, but was neither allowed to overlap with the stacking aperture of an optical source position, nor allowed to lie within three times the 90 per cent encircled-energy fraction radius of an X-ray detected source. The Monte Carlo procedure was carried out 10 000 times (except during the stacking of all the sources in the catalogue, where only 1000 trials were computationally feasible due to the large number of sources; see Table 3), and the mean and variance of the background level determined.

We quantify the significance of the detection of X-ray emission from the stacked objects in terms of the S/N. This is given by

$$\mathrm{S/N} = \frac{S - B}{\sqrt{B}}, \tag{1}$$

where S is the total number of stacked-source counts (i.e sources and background) and B is the total number of Monte Carlo stacked-background counts (i.e. background only). For the ease of reference, Table 1 gives the probability of a false detection (i.e. the probability of recording the excess counts above background by chance alone), for various S/Ns.

Total count-rates were derived by dividing the total number of stacked counts by the total stacked exposure time. These were then

[1] Available at http://www.stsci.edu/science/goods/.

Table 1. The probability, $P_{\rm false}(\sigma)$, of falsely recording a given S/N, σ, in the stacking signal due to background fluctuations alone, when no sources are actually present. The probability of a genuine detection is thus $1 - P_{\rm false}(\sigma)$. The values correspond to the one-tailed integrated Gaussian probabilities, that is, $P_{\rm false}(\sigma) = (2\pi)^{-1/2} \int_{\sigma}^{\infty} \exp(-x^2/2)\,{\rm d}x$.

S/N (σ)	$P_{\rm false}$
0.5	0.309
1	0.159
1.5	0.0668
2	0.0228
3	1.35×10^{-3}
4	3.17×10^{-5}
5	2.87×10^{-7}

converted to fluxes using counts-to-flux conversion factors from Alexander et al. (2003a). We assumed a $\Gamma = 1.4$ power law plus Galactic absorption of $N_{\rm H} = 1.3 \times 10^{20}$ and $8.8 \times 10^{19}\,{\rm cm}^{-2}$ for the CDF-N (Lockman 2004) and CDF-S (Stark et al. 1992), respectively. The conversion factors are given in Table 2 and include the necessary corrections for Galactic absorption and the low-energy absorption seen in *Chandra* due to molecular contamination of the telescope's optical blocking filters.

The size of the *Chandra* point spread function (PSF) varies strongly with off-axis angle. The radius enclosing 50 per cent of the counts from a point-source is only $\lesssim$0.5 arcsec at the aim-point rising to $\gtrsim$4 arcsec at an off-axis angle of 10 arcmin (at 1.5 keV). Since the sky density of the optical sources is high enough to result in overlap of the PSFs towards the edges of the fields, we restricted our analysis to the central 4.5 arcmin of the X-ray field to avoid confusion between sources, and between sources and background. Stacking sources in these central regions also enabled the use of a 3 pixel fixed aperture size, which encloses the core of the PSF. The PSF remains fairly compact, and more importantly, well measured over these central regions and so the stacked counts can be easily corrected for PSF effects. We used the data[2] from a circular parametrization of the PSF in order to calculate and correct for the encircled-energy fraction at each aperture position and energy band. The average encircled energy fractions in each of the energy bands for the CDF-N and CDF-S are given in Table 2.

The total stacked-source fluxes were finally converted to intensity over the solid angle on the sky in which the sources were stacked; in this case this is simply the circular central 4.5-arcmin region ($\sim$63.6 arcmin^2), minus the area of the regions around X-ray detected sources which we excluded from our analysis. The excluded solid angles are 6.6 and 4.3 arcmin^2 in the CDF-N and CDF-S, respectively.

2.3 XRB model

In order to calculate the fraction of the XRB which can be attributed to the stacked sources, we assume the XRB spectrum from Worsley et al. (2005). This is a 1–8 keV power law of photon index $\Gamma = 1.41$ and with a 1-keV normalization of 11.6 keV cm^{-2} s^{-1} sr^{-1} keV^{-1} as observed by De Luca & Molendi (2004). Above 8 keV the analytical model of Gruber et al. (1999) is used, although re-normalized to smoothly intercept the 1–8 keV power law. Below 1 keV we use a steeper power law ($\Gamma \sim 1.6$), which intercepts the low-energy extragalactic XRB measurements from Roberts & Warwick (2001).

Whilst the slope of the XRB is well known in the 1–8 keV range, the normalization measured by different instruments shows 5–10 per cent variations. These measurements (see e.g. Vecchi et al. 1999; Lumb et al. 2002; Revnivtsev et al. 2003; De Luca & Molendi 2004) are typically obtained over large regions, typically several square degrees. The variations in XRB normalization can be explained in terms of uncertainties in the cross-calibration between instruments, and the field-to-field variations arising from the discrete nature of the sources making up the background. In pencil-beam fields such as the CDFs, which only sample $\lesssim$0.1 deg^2, field-to-field variations are at least 10 per cent (Barcons et al. 2000), and further variations could be due to true 'cosmic variance' – real differences in XRB level beyond those simply arising due to sampling statistics. For example, spatial clustering on the sky (see e.g. Gilli et al. 2003, 2005) could be responsible for additional variations in normalization, whilst clustering in redshift space could create additional variations in XRB spectral shape. Error in our XRB spectrum is taken from the measurement errors quoted for the different sources: we have not added any additional uncertainty to allow for field-to-field variations.

Table 2. Counts-to-flux conversion factors for the CDF-N and CDF-S data. The factors convert source count-rate (count s^{-1}) to flux (erg cm^{-2} s^{-1}) and were computed assuming a $\Gamma = 1.4$ power-law spectrum inclusive of Galactic absorption. The factors include the Galactic absorption correction and also take into account the effects of absorption due to the *Chandra* molecular contamination. (See Alexander et al. 2003a for details.) The encircled energy fractions give the average fraction of source counts lying within the stacking aperture in each of the energy bands for the CDF-N and CDF-S. The values given were calculated using for the 'all sources' cases with a 3-pixel (1.476-arcsec) radius aperture.

Energy band (keV)	Counts-to-flux conversion factor (10^{-11} erg cm^{-2} count^{-1})		Encircled energy fraction (3-pixel radius aperture)	
	CDF-N	CDF-S	CDF-N	CDF-S
0.5–1	0.691 86	0.653 27	0.705	0.704
1–2	0.443 69	0.463 58	0.690	0.688
2–4	1.4583	1.5830	0.653	0.652
4–6	2.4763	2.7689	0.612	0.612
6–8	8.9967	10.254	0.567	0.567

3 RESULTS AND DISCUSSION

3.1 Optical source-stacking

Table 3 summarizes our stacking analyses of the optically-detected GOODS sources. The CDF-N and CDF-S fields were stacked separately to provide robustness. Stacking of all the optical sources in the fields revealed highly significant ($\sim$10–30σ) detections in the soft 0.5–1 and 1–2 keV bands. Strong results are seen in the 2–4 keV band (7.3 and 7.8σ for the CDF-N and CDF-S fields, respectively) and the broad 2–8 keV range (4.5 and 6.5σ). Detection of flux in the very hard 4–6 keV band is tentative at 2.6 and 2.0σ, although the combined CDF-N and CDF-S detection is significant at the $\sim$99 per cent level. No significant detection is found in the 6–8 keV

[2] *Enclosed Count Fractions (ECF) using circular apertures based on the SAOsac model of the Chandra PSF* (2005 June 24) which is available at http://cxc.harvard.edu/cal/Hrma/psf/ECF/hrmaD1996-12-20hrci_ecf_N0002.fits.

Table 3. The results of stacking the emission from the optically-detected, but individually X-ray undetected, GOODS sources. For the CDF-N and CDF-S analyses, the results are shown for each of the different energy bands and also for the different z_{850}-band magnitude selections applied to the sources included in the stacking. If an excess of X-ray counts was detected, then the detection S/N is quoted; '–' indicates non-detection, that is, S/N < 0.

	Energy band (keV)	S/N (σ)						
CDF-N sources:		$z_{850} < 21$	$z_{850} < 22$	$z_{850} < 23$	$z_{850} < 24$	$z_{850} < 25$	$z_{850} < 26$	All sources
Number stacked:		117	278	571	1160	2132	3720	10 052
	0.5–1	10.1	13.8	15.9	17.1	17.1	16.2	14.6
	1–2	10.8	20.0	26.4	28.2	31.1	29.8	27.6
	2–4	6.8	8.2	9.7	8.4	7.7	8.3	7.3
	4–6	2.3	2.9	4.3	3.2	3.1	3.2	2.6
	6–8	–	–	1.2	1.0	0.4	0.2	–
CDF-S sources:		$z_{850} < 21$	$z_{850} < 22$	$z_{850} < 23$	$z_{850} < 24$	$z_{850} < 25$	$z_{850} < 26$	All sources
Number stacked:		128	289	537	1034	1913	3426	9599
	0.5–1	9.4	9.9	10.6	11.5	11.7	12.2	10.1
	1–2	13.7	17.8	20.3	21.9	23.4	23.3	22.2
	2–4	3.8	5.4	5.6	7.7	8.7	6.7	7.8
	4–6	1.7	1.4	2.1	1.7	2.8	1.5	2.0
	6–8	1.5	1.9	0.7	–	0.5	0.7	1.1

band with only a 1.1σ signal in the CDF-S and a non-detection (i.e. S/N < 0) in the CDF-N. We would also note that we see no obvious evidence for any spatial extension of the X-ray emission in the X-ray images associated with the stacking analysis, although a more complete investigation would be needed to pursue this further.

We repeated the stacking analyses using subsamples of the GOODS sources, selecting on the z_{850}-band, which samples the ∼8300–9500 Å wavelength range. The publicly available GOODS catalogue is z_{850}-band selected. The strongest detection of a soft (0.5–2 keV) X-ray signal occurs for the $z_{850} \lesssim 25$ galaxies, whilst the highest S/N of hard X-ray signals tends to occur for the brighter subsamples, although the detections are borderline except for a 4–6 keV signal at 4.3σ for the CDF-N with $z_{850} < 23$ sources. There is also hint of a 6–8 keV signal for the CDF-N with $z_{850} < 23$ sources (1.2σ), and the CDF-S with $z_{850} < 22$ sources (1.9σ). For the individual sources, we plotted X-ray counts against optical flux in various bands, but saw no obvious correlation, nor was there any obvious trend apparent in similar plots of X-ray flux against various optical colours.

3.2 Source contributions to the unresolved XRB

Table 4 shows the total flux due to the stacked sources expressed as a percentage of the total XRB level (refer to Section 2.3 for details of the XRB model assumed). Around ∼15–20 per cent of the 0.5–4 keV background is contributed by the GOODS sources. In the 4–6 keV band the contribution is ∼10 ± 5 per cent. However, only a 3σ upper limit of 82 per cent can be placed on the 6–8 keV contribution using the CDF-N, with the CDF-S indicating 32 ±

Table 4. The percentage of the total XRB flux in the signal from stacking the optically-detected, but individually X-ray undetected, GOODS sources. For the CDF-N and CDF-S analyses, the results are shown for each of the different energy bands and also for the different z_{850}-band magnitude selections applied to the sources included in the stacking. In the case of non-detection (i.e. S/N < 0), a 3σ upper limit is given. The 'Already resolved' column indicates the fraction of the XRB which has already been accounted for by X-ray detected sources (see Worsley et al. 2005).

	Energy band (keV)	Percentage of XRB flux							
CDF-N sources:		$z_{850} < 21$	$z_{850} < 22$	$z_{850} < 23$	$z_{850} < 24$	$z_{850} < 25$	$z_{850} < 26$	All sources	Already resolved
Number stacked:		117	278	571	1160	2132	3720	10 052	
	0.5–1	1.4 ± 0.3	2.8 ± 0.4	4.6 ± 0.7	7.1 ± 1.0	9.6 ± 1.3	12.1 ± 1.6	17.7 ± 2.5	86 ± 11
	1–2	0.8 ± 0.1	2.1 ± 0.2	4.0 ± 0.3	6.1 ± 0.4	9.1 ± 0.5	11.5 ± 0.7	17.3 ± 1.0	83 ± 5
	2–4	1.3 ± 0.3	2.3 ± 0.5	3.9 ± 0.7	5.0 ± 0.9	6.2 ± 1.2	8.8 ± 1.6	12.6 ± 2.6	91 ± 8
	4–6	0.9 ± 0.6	1.7 ± 0.9	3.5 ± 1.2	3.8 ± 1.8	5.0 ± 2.3	6.8 ± 3.1	9.2 ± 5.1	92 ± 13
	6–8	<8.9	<13.2	5.2 ± 6.3	6.4 ± 9.2	3.2 ± 12.4	1.9 ± 16.4	<81.9	56 ± 12
CDF-S Sources:		$z_{850} < 21$	$z_{850} < 22$	$z_{850} < 23$	$z_{850} < 24$	$z_{850} < 25$	$z_{850} < 26$	All sources	Already resolved
Number stacked:		128	289	537	1034	1913	3426	9599	
	0.5–1	1.9 ± 0.4	3.0 ± 0.6	4.5 ± 0.8	6.6 ± 1.1	9.0 ± 1.5	12.7 ± 2.0	17.4 ± 3.1	74 ± 9
	1–2	1.4 ± 0.2	2.8 ± 0.3	4.3 ± 0.4	6.4 ± 0.5	9.2 ± 0.7	12.1 ± 0.9	19.1 ± 1.4	72 ± 5
	2–4	1.1 ± 0.5	2.4 ± 0.7	3.4 ± 0.9	6.4 ± 1.3	9.7 ± 1.8	10.0 ± 2.3	19.4 ± 3.8	83 ± 7
	4–6	1.0 ± 0.9	1.2 ± 1.3	2.7 ± 1.8	3.0 ± 2.5	6.5 ± 3.4	4.7 ± 4.4	10.5 ± 7.4	82 ± 11
	6–8	5.4 ± 5.1	9.9 ± 7.6	5.3 ± 10.4	<42.1	6.8 ± 18.9	12.6 ± 25.3	32.4 ± 42.3	66 ± 11

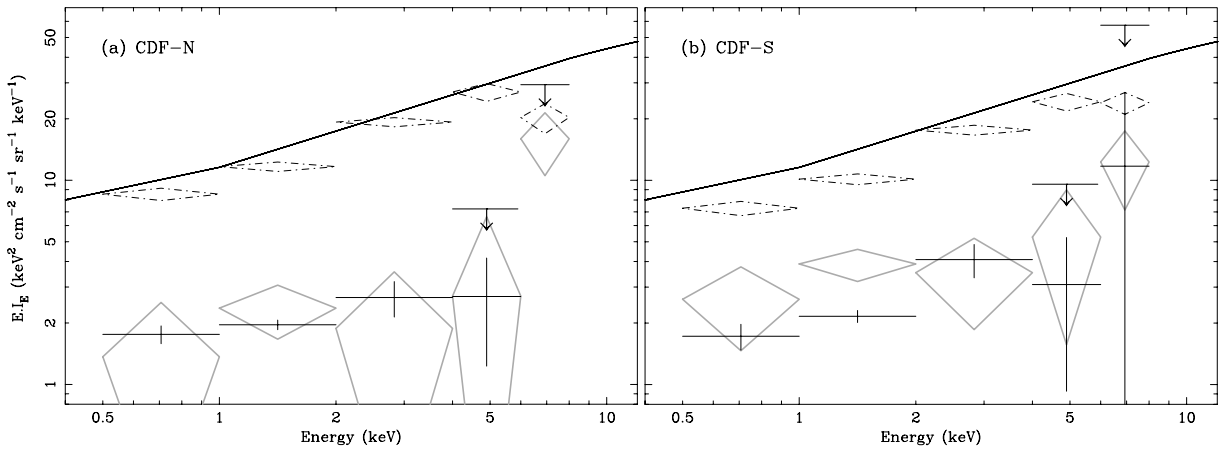

Figure 1. The extragalactic XRB with the resolved and stacked contributions. The panels (a) and (b) show the data for the CDF-N and CDF-S, respectively. In each case the solid black line shows the total XRB level and the broken black diamonds show the intensity resolved from individually detected X-ray sources (see Introduction and Worsley et al. 2005). The grey diamonds indicate the missing intensity, that is, the residual remaining once the resolved contributions are subtracted from the total XRB level. The solid black crosses now indicate the stacked intensity due to the optically-detected, but individually X-ray undetected, GOODS sources determined in this work. Additionally, for the 4–6 and 6–8 keV bands, 3σ upper limits to the stacked intensity are shown.

42 per cent. Both measurements are consistent with both zero and a large contribution in this range.

Fig. 1 shows the spectral shape of the stacked X-ray emission from the GOODS sources, and the relative contributions to the total XRB level. It is encouraging to note that (at least for the <6 keV range) we find the stacked contribution to the XRB agrees well with the 'missing' intensity, once that from X-ray detected sources has been considered. The large errors mean that there remains some room for other emission, particularly in the 0.5–2 keV band, even when a ∼6 per cent contribution from clusters is taken into account (see e.g. Moretti et al. 2003). The residual emission can place important constraints on any truly diffuse components (Sołtan 2003) and the total contribution of accreting black holes to reionization (Dijkstra, Haiman & Loeb 2004), but it is difficult to place any limits on the still-unresolved emission, given the large errors and without a more thorough understanding of cosmic variance.

The reduction in the sensitivity of *Chandra* above 6 keV means that the instrumental background heavily outweighs any source signal and errors in the stacked X-ray intensity become very large. In the CDF-N 6–8 keV band, the detection of a stacked signal representing ∼40 per cent of the total XRB – the full unresolved intensity in this band – would only correspond to a S/N $\sim 2.1\sigma$ (S/N $\sim 1.4\sigma$ in the CDF-S), with background counts exceeding source counts by a factor of ∼100. The 3σ upper limit of 82 per cent to the CDF-N stacked intensity is easily consistent with what is required to account fully for the background. The CDF-S stacked intensity gives 32 ± 42 per cent, although the error is again very large. The 3σ upper limit in the CDF-S exceeds 100 per cent.

Since the GOODS will detect $L_\star$ galaxies out to redshift $z \sim 6$, we would expect the optically-detected sources to include almost every galaxy capable of hosting a significant AGN. Although the stacked X-ray flux from the GOODS optical sources is consistent with the missing XRB intensity, it is still possible that the contribution could be much lower and we briefly discuss the possible source populations which may be missing from our analysis. If the actual contribution is indeed much less than that is needed to explain the unresolved XRB, then the missing AGN must come from rare sources, occurring with sky densities $\lesssim 10\,\mathrm{deg}^{-2}$ and so not sampled well in the pencil-beam surveys; or, from very faint galaxies that are not optically-detected in the GOODS.

3.2.1 Rare source populations

The first of these possibilities requires the missing AGN to occur with sky densities $\lesssim 10\,\mathrm{deg}^{-2}$, therefore not sampled by the $\sim 0.1\,\mathrm{deg}^2$ deep surveys, and explaining why the stacked source emission fails to account for ∼40 per cent of the 6–8 keV XRB emission. However, it is also clear that the missing sources must occur with sky densities $\gtrsim 1\,\mathrm{deg}^{-2}$. This is because total XRB emission measurements by De Luca & Molendi (2004), who analysed the background in the fields of $\sim 5.5\,\mathrm{deg}^2$ of the *XMM–Newton* observations, found the total XRB emission is a $\Gamma = 1.4$ power law up to at least 8 keV. The missing AGN must therefore be present at $\gtrsim 1\,\mathrm{deg}^{-2}$ in order to be present in their analysis and provide the full XRB flux.

At densities of $1\text{–}10\,\mathrm{deg}^{-2}$, in order to be responsible for the full ∼40 per cent of unresolved 6–8 keV XRB, the required flux per source would need to be $\gtrsim 2 \times 10^{-13}\,\mathrm{erg\,cm^{-2}\,s^{-1}}$ in this band. Since only ∼10 per cent of the 4–6 keV band is unresolved (Worsley et al. 2005), the required sources need to be Compton thick with $N_\mathrm{H} \gtrsim 2 \times 10^{24}\,\mathrm{cm}^{-2}$ (to have a negligible $\lesssim 6$ keV contribution) and of quasar luminosity ($L_{2-10\,\mathrm{keV}} \gtrsim 5 \times 10^{44}$). Whilst Gandhi et al. (2004) have found several type II quasi-stellar objects (QSOs) serendipitously at sky densities of $\gtrsim 10\,\mathrm{deg}^{-2}$, their sources tend to have $N_\mathrm{H} = 10^{23}\text{–}10^{24}\,\mathrm{cm}^{-2}$ and the contribution to the XRB in the 6–8 keV band is only a few per cent.

3.2.2 Optically-undetected sources

The second alternative – that AGN hosts could remain optically-undetected – is supported by the discovery of extreme X-ray/optical sources (EXOs) which show X-ray fluxes of $\sim 10^{-16}\text{–}10^{-15}\,\mathrm{erg\,cm^{-2}\,s^{-1}}$, yet are optically-undetected with $z_{850} \gtrsim 28$ (Koekemoer et al. 2004a). The 7 EXOs in the CDF-S have now been detected using the 24-μm *Spitzer* observations (Koekemoer et al. 2004b). Interestingly, Wang et al. (2004) found that several of the EXOs show very hard X-ray spectra, consistent with type II AGN at redshift $\lesssim 6$ hosted by very underluminous, or very dusty galaxies. It is plausible that X-ray undetected EXOs may contribute a few per cent to the total XRB level (those identified to date in the CDF-S contribute ∼0.5–1.5 per cent).

3.3 Spectral shape: AGN and starburst components

The softer $\lesssim$4 keV flux seen from the GOODS sources is most likely to be dominated by starburst emission in these faint galaxies with a photon index $\Gamma \sim 1.5$–2. The average 0.5–2 keV flux of the GOODS sources is $\sim 2 \times 10^{-18}$ erg cm^{-2} s^{-1} at a sky density of $\sim 6 \times 10^5$ deg^{-2}. Adding this point to a soft X-ray $\log N$–$\log S$ diagram (see fig. 4 in Bauer et al. 2004) is consistent with a direct extrapolation of the steeply climbing number-counts distribution of star-forming galaxies, which at these very faint fluxes, outnumber AGN by an order of magnitude. Starburst activity is a likely explanation for the $\lesssim$4 keV stacked emission, although weak AGN activity is also possible.

Worsley et al. (2005) modelled the missing hard XRB intensity as emission from a population of heavily obscured AGN: a simplified spectral model consisting of a $\Gamma = 2$ power law, plus photoelectric absorption and a reflection component, is able to explain the shape of the missing >2 keV XRB emission inferred from the *Chandra* Deep Fields for redshifts $\sim$0.5–1 and column densities $\sim 10^{23}$–5×10^{24} cm^{-2} (see fig. 4 in Worsley et al. 2005). Within the errors, the stacked X-ray emission from the GOODS sources does have a spectral shape which is consistent with that predicted from obscured AGN activity.

Assuming that the missing hard XRB can be explained by the hypothesized population of obscured AGN, the difficulty is in reducing the error in the 6–8 keV stacked *Chandra* emission to the point where definite verification or inconsistency can be seen between the XRB residual and the stacked GOODS intensity. If, for example, only 10 per cent of the GOODS galaxies contain an obscured AGN, then the overwhelming majority of stacked X-ray positions are simply adding background noise to the measurement; we need to be able to select the likely AGN candidates. Our attempt to do this on the basis of the z_{850}-band optical magnitude was not successful, with no particular z_{850}-band magnitude restriction improving the 6–8 keV signal over that obtained when all sources were included, although there is a weak improvement when only the brighter ($z_{850} \lesssim 24$) objects are selected. Selections of $z_{850} \lesssim 23$–25 did, however, succeed in increasing the S/N of the 4–6 keV band considerably: from 2.6 to 4.3σ in the CDF-N ($z_{850} \lesssim 23$); and from from 2.0 to 2.8σ in the CDF-N ($z_{850} \lesssim 25$A).

A much better method of discrimination could be the use of IR fluxes which will soon be available from *Spitzer* observations. Highly absorbed AGN are expected to show strong far-IR emission due to the reprocessing of X-ray emission by the obscuring dust. The difficulty here would be separating the obscured AGN candidates from strong starburst galaxies, which are also bright in the IR.

4 CONCLUSIONS

We have stacked the emission from X-ray undetected optical sources in the GOODS fields to address the question of whether they can account for the missing hard XRB implied by the stacking of X-ray detected sources (Worsley et al. 2005). Our central conclusion is 'plausibly, but not certainly, yes'. Whilst X-ray emission is detected at high significance in the 0.5–4 keV range, the strong downturn in the *Chandra* sensitivity makes detection more difficult at higher energies. By selecting the sources on the basis of z_{850}-band (8300–9500 Å) magnitude, we were able to obtain 4.3 and 2.8σ detections of 4–6 keV emission in the CDF-N and CDF-S fields, respectively, whilst in the 6–8 keV band we only achieve constraints at the 1.2 and 1.9σ levels, respectively.

The 0.5–4 keV emission represents some 15–20 per cent of the XRB with $\sim 10 \pm 5$ per cent in the 4–6 keV band. When added to the fractions due to the resolved XRB the totals are consistent with 100 per cent, although depending on XRB normalization (and spectral shape <1 keV), there remains room for contributions from other sources. The CDF-S 6–8 keV intensity is 32 ± 42 per cent, suggesting that at least half of the unresolved XRB ($\sim$40 per cent), may be lurking in these sources; however, the errors are considerable, and the CDF-N shows no clear excess in the stacked 6–8 keV intensity above the instrumental background, although the 3σ upper limit to the potential XRB contribution is 82 per cent in the CDF-N, which is more than enough to account for the unresolved intensity.

In previous work, we predicted that the missing component of the XRB is due to moderate luminosity, highly obscured AGN, with absorption column densities of $\sim 10^{23}$–5×10^{24} cm^{-2}, at redshift $\sim$0.5–1.5. Since the GOODS is able to detect $L_\star$ galaxies out to a redshift $z \sim 6$, we expected it to include the hosts of this heavily obscured AGN population. The stacked X-ray flux in the CDF-S shows a larger contribution in the 6–8 keV band (see Fig. 1), precisely where the steeply rising spectrum of these sources becomes important. This could be the sought-after signature of the missing population, although the poor S/N and the consequently large errors mean the detection is uncertain.

Our results are also consistent with a negligible additional contribution to the XRB in the 6–8 keV band, which if true, would imply that the highly obscured AGN population is hosted by galaxies which are optically-undetected in the GOODS fields. Even with the recent discovery of EXOs, it seems unlikely that such a large AGN population can be accommodated by such optically faint hosts. A strong contribution could also be due to Compton thick quasars occurring with sky densities of 1–10 deg^{-2}.

In order to boost the S/N of the stacked GOODS signal, there remains much work to be done in selecting the appropriate subsample of sources, and avoid adding background noise to the measurement by including ordinary galaxies. IR-bright galaxies identified by *Spitzer* may hold the key to doing this, assuming differentiation between dusty star-forming galaxies, and potential obscured AGN, can be accomplished. Additional deep-field observations, particularly further exposure in the CDF-N, could resolve the situation by increasing the sensitivity to individual, faint X-ray sources, as well as improve the S/N in stacked-source signals in the hardest energy bands. Additional investigations into EXOs will also provide useful constraints, as will shallow wide-area surveys at hard X-ray energies, which can place important limits on the contribution from heavily obscured quasars.

As a final comment we note that there is good agreement with the recent work of Hickox & Markevitch (2006) where both the resolved sources and unresolved background are measured in the 0.5–8 keV band using *Chandra* in the Deep Fields. The total background they determine has a normalization 6 per cent less than we assume (Section 2.3), but with an uncertainty of 11 per cent. A large amount of the difference in normalizations is probably due to differences in analysis methods, the most significant of which is our 'bright-end correction' (see Worsley et al. 2005) which attempts to correct for the poor sampling of the bright end of the X-ray number counts distribution. The resolved fractions found by Hickox & Markevitch are in good agreement with our results in the bands used (1–2 and 2–8 keV).

ACKNOWLEDGMENTS

MAW and FEB acknowledge support from the PPARC. ACF and DMA thank the Royal Society for support. WNB and BDL thank

the NSF career award AST-9983783 and CXC grant GO4-5157 for support. MAW would like to thank his coauthors for their support and patience in seeing this work through to publication.

REFERENCES

Alexander D. M. et al., 2003a, AJ, 126, 539
Alexander D. M. et al., 2003b, AJ, 125, 383
Alexander D. M., Smail I., Bauer F. E., Chapman S. C., Blain A. W., Brandt W. N., Ivison R. J., 2005, Nat, 434, 738
Alonso-Herrero A. et al., 2004, ApJS, 154, 155
Baldi A., Molendi S., Comastri A., Fiore F., Matt G., Vignali C., 2002, ApJ, 564, 190
Barcons X., Mateos S., Ceballos M. T., 2000, MNRAS, 316, L13
Bauer F. E., Alexander D. M., Brandt W. N., Schneider D. P., Treister E., Hornschemeier A. E., Garmire G. P., 2004, AJ, 128, 2048
Brandt W. N., Hasinger G., 2005, ARA&A, 43, 827
Brandt W. N., Hornschemeier A. E., Schneider D. P., Alexander D. M., Bauer F. E., Garmire G. P., Vignali C., 2001, ApJ, 558, L5
Comastri A., 2004, in Mújica R., Maiolino R., eds, Proc. Guillermo Haro Conf. Multiwavelength AGN Surveys. World Scientific, Singapore, p. 323
De Luca A., Molendi S., 2004, A&A, 419, 837
Dickinson M., Giavalisco M., The GOODS Team, 2003, in Bender R., Renzini A., eds, The Mass of Galaxies at Low and High Redshift. Springer-Verlag, Heidelberg, p. 324
Dijkstra M., Haiman Z., Loeb A., 2004, ApJ, 613, 646
Ferguson H. C., Dickinson M., Williams R., 2000, ARA&A, 38, 667
Fiore F. et al., 2003, A&A, 409, 79
Franceschini A., Braito V., Fadda D., 2002, MNRAS, 335, L51
Gandhi P., Fabian A. C., 2003, MNRAS, 339, 1095
Gandhi P., Crawford C. S., Fabian A. C., Johnstone R. M., 2004, MNRAS, 348, 529
Giacconi R. et al., 2002, ApJS, 139, 369
Giavalisco M. et al., 2004, ApJ, 600, L93
Gilli R., Salvati M., Hasinger G., 2001, A&A, 366, 407
Gilli R. et al., 2003, ApJ, 592, 721
Gilli R. et al., 2005, A&A, 430, 811
Gruber D. E., Matteson J. L., Peterson L. E., Jung G. V., 1999, ApJ, 520, 124
Hasinger G. et al., 2001, A&A, 365, L45
Hickox R. C., Markevitch M., 2006, ApJ, submitted (astro-ph/0512542)
Koekemoer A. M. et al., 2004a, ApJ, 600, L123
Koekemoer A. M. et al., 2004b, 205th American Astronomical Society Meeting Abstracts, Session 62, Poster 13
Lacy M. et al., 2004, ApJS, 154, 166
Lacy M., Canalizo G., Rawlings S., Sajina A., Storrie-Lombardi L., Armus L., Marleau F. R., Muzzin A., 2005, Memorie Soc. Astron. Italiana, 76, 154
Lehmer B. D., 2005, AJ, 129, 1
Lockman F. J., 2004, in Lieu R., Mittaz J., eds, Soft X-ray Emission from Clusters of Galaxies and Related Phenomena. Kluwer, Dordrecht, p. 111
Lumb D. H., Warwick R. S., Page M., De Luca A., 2002, A&A, 389, 93
Matt G., Fabian A. C., Guainazzi M., Iwasawa K., Bassani L., Malaguti G., 2000, MNRAS, 318, 173
Moretti A., Campana S., Lazzati D., Tagliaferri G., 2003, ApJ, 588, 696
Mushotzky R. F., Cowie L. L., Barger A. J., Arnaud K. A., 2000, Nat, 404, 459
Nandra K., Mushotzky R. F., Arnaud K., Steidel C. C., Adelberger K. L., Gardner J. P., Teplitz H. I., Windhorst R. A., 2002, ApJ, 576, 625
Norman C. et al., 2002, ApJ, 571, 218
Revnivtsev M., Gilfanov M., Sunyaev R., Jahoda K., Markwardt C., 2003, A&A, 411, 329
Roberts T. P., Warwick R. S., 2001, in Giacconi R., Salvatore S., Luigi S., eds, ASP Conf. Ser. Vol. 234, X-ray Astronomy 2000. Astron. Soc. Pac., San Francisco, p. 569
Rosati P. et al., 2002, ApJ, 566, 667
Setti G., Woltjer L., 1989, A&A, 224, L21
Sołtan A. M., 2003, A&A, 408, 39
Stark A. A., Gammie C. F., Wilson R. W., Bally J., Linke R. A., Heiles C., Hurwitz M., 1992, ApJS, 79, 77
Stern D. et al., 2002, ApJ, 568, 71
Streblyanska A., Bergeron J., Brunner H., Finoguenov A., Hasinger G., Mainieri V., 2004, Nuclear Physics B Proceedings Supplements, 132, 232
Treister E. et al., 2004, ApJ, 616, 123
Ueda Y., Takahashi T., Ishisaki Y., Ohashi T., Makishima K., 1999, ApJ, 524, L11
Ueda Y., Akiyama M., Ohta K., Miyaji T., 2003, ApJ, 598, 886
Vecchi A., Molendi S., Guainazzi M., Fiore F., Parmar A. N., 1999, A&A, 349, L73
Wang J. X., Malhotra S., Rhoads J. E., Norman C. A., 2004, ApJ, 612, L109
Williams R. E. et al., 1996, AJ, 112, 1335
Worsley M. A., Fabian A. C., Barcons X., Mateos S., Hasinger G., Brunner H., 2004, MNRAS, 352, L28
Worsley M. A. et al., 2005, MNRAS, 357, 1281

This paper has been typeset from a TEX/LATEX file prepared by the author.